Cosserat crystal plasticity with dislocation driven grain boundary migration

Anna Ask, Samuel Forest, Benoît Appolaire, Kais Ammar

Cosserat crystal plasticity with dislocation driven grain boundary migration

Anna Ask

MINES ParisTech, PSL Research University, MAT – Centre des matériaux, CNRS UMR 7633 BP 87 91003 Evry, France

Samuel Forest*

MINES ParisTech, PSL Research University, MAT – Centre des matériaux, CNRS UMR 7633 BP 87 91003 Evry, France

Benoit Appolaire

Institut Jean Lamour, Université de Lorraine, 2 allée André Guinier 54000 Nancy, France

Kais Ammar

MINES ParisTech, PSL Research University, MAT – Centre des matériaux, CNRS UMR 7633 BP 87 91003 Evry, France

Received date
Accepted date

Abstract This paper discusses a coupled mechanics–phase field model that can predict microstructure evolution in metallic polycrystals and in particular evolution of lattice orientation due to either deformation or grain boundary migration. The modeling framework relies on the link between lattice curvature and geometrically necessary dislocations and connects a micropolar or Cosserat theory with an orientation phase field model. Some focus is placed on the underlying theory and in particular the theory of dislocations within a continuum single crystal plasticity setting. The model is finally applied to the triple junction problem for which there is an analytic solution if the grain boundary energies are known. The attention is drawn on the evolution of skew–symmetric stresses inside the grain boundary during migration.

Keywords Crystal plasticity; Cosserat; Non-local theory; Phase field method; Dislocation Density Tensor.

1. Introduction

By controlled thermomechanical processing, the microstructure of metallic polycrystals can be manipulated in order to obtain certain desired material properties. A typical example is cold working followed by annealing, where energy is stored in the material during viscoplastic deformation and later released by nucleation and growth of new grains. Deformation at elevated temperatures on the other hand may lead to concurrent (dynamic) recrystallization [Humphreys and Hatherly, 2004].

*Corresponding author: samuel.forest@ensmp.fr

Simulation models for microstructure evolution in metals can be formulated at length scales from the atomistic up to the continuum level. Models at the lower scales (atomistic simulations, molecular dynamics) are computationally demanding due to their very high resolution and not feasible for polycrystals undergoing load sequences which may last minutes or hours. On the other hand, a macroscopic model which retains no information about the microstructure is too coarse. The most promising models are therefore formulated at the mesoscopic level, resolving the grain structure but not individual atoms, defects or dislocations. Several authors have developed approaches which rely on coupling on the one hand continuum single crystal plasticity and on the other hand numerical methods for nucleation and/or grain boundary motion (a by no means exhaustive list of examples is e.g. [Abrivard *et al.*, 2012a; Mellbin *et al.*, 2017; Takaki *et al.*, 2007; Takaki and Tomita, 2010; Raabe and Becker, 2000; Güvenç *et al.*, 2013, 2014; Blesgen, 2017; Chuan *et al.*, 2013; Vondrous *et al.*, 2015]). Information is passed between the separate models which are solved in individual steps. While these sequentially coupled models can be very successful for certain applications, they do not represent a unified, thermodynamically consistent theory of microstructure evolution in polycrystals. Recently, Ask *et al.* [2018b] and Admal *et al.* [2018] have proposed such strongly coupled models based on higher order single crystal plasticity theories and an orientation phase field method originally introduced by Kobayashi *et al.* [2000]; Warren *et al.* [2003]. Orientation phase field models are well suited for coupling with crystal plasticity models as they rely on a continuous representation of lattice orientation both at grain boundaries and inside the grains. This is in contrast to methods that rely on a cellular description of the microstructure with constant orientation within each cell or grain, such as Monte-Carlo-Potts models, cellular automata or vertex models [Rollett, 1997; Gottstein and Shvindlerman, 2010].

The coupled crystal plasticity-phase field approach proposed by Admal *et al.* [2018] relies on a strain gradient plasticity approach in the spirit of [Cermelli and Gurtin, 2001; Gurtin, 2002]. A non-standard free energy function based on a phase field order parameter and the tensor of so called geometrically necessary dislocations is formulated inspired by the orientation phase field model of [Kobayashi *et al.*, 2000; Warren *et al.*, 2003]. This results in a model capable of predicting grain boundary migration on the one hand due to capillary forces (grain boundary curvature) and on the other hand due to shear-induced grain boundary motion and grain sliding. The formulation relies on introducing the plastic slips on each slip system as kinematic variables with their own associated microstress balances and the representation of grain boundaries in terms of geometrically necessary dislocations. Grain boundary motion in the model by Admal *et al.* [2018] is accommodated by plastic slip processes.

In the present work a coupled crystal plasticity-phase field model introduced by Ask *et al.* [2018b] is revisited. In order to take into account non-local effects, a Cosserat or micropolar [Cosserat and Cosserat, 1909; Eringen and Kafadar, 1976;

Eringen, 1976; Forest *et al.*, 1997] approach is adopted and the lattice orientation changes of the crystal are associated on the constitutive level with the Cosserat microrotations, which enter as additional degrees of freedom. It was shown in Ask *et al.* [2018b] that such a modeling approach allows evolution of lattice orientation at a material point both due to viscoplastic deformation and grain boundary migration. The considered driving forces for grain boundary migration were capillary forces as well as stored energy due to scalar dislocation densities accumulated during deformation. The model allows for reorientation of the crystal lattice due to plastic slip processes but grain boundary migration mechanism is not associated directly with plastic slip. A linearized version of the model by Ask *et al.* [2018a] is used in this work and applied to the solution of the triple junction problem where three grains meet at a common point. The objective is to study the development and relaxation of skew–symmetric stresses predicted by the model in the moving grain boundaries and at the triple junction.

This article is structured as follows. The first two sections discuss important aspects of the phase field method and crystal plasticity theory, respectively. The third section presents the coupled Cosserat crystal plasticity-phase field framework. This is followed by a section dedicated to the numerical solution of the called triple junction problem. The paper is concluded with a summary of the presented theory and the outlook for future work.

Notation

Vectors and second order tensors are denoted by $\underline{\boldsymbol{a}}$ and $\underset{\sim}{\boldsymbol{A}}$, with the transpose $\underset{\sim}{\boldsymbol{A}}^T$. Third order tensors are given by $\underset{\approx}{\boldsymbol{a}}$ and fourth order tensors by $\underset{\approx}{\boldsymbol{C}}$. In particular, $\underset{\sim}{\boldsymbol{I}}$ is the second order identity tensor and $\underset{\approx}{\boldsymbol{\epsilon}}$ is the third-order Levi-Civita permutation tensor. The latter is used to express skew-symmetric tensors as pseudo-vectors

$$\overset{\times}{\underline{\boldsymbol{A}}} = -\frac{1}{2}\underset{\approx}{\boldsymbol{\epsilon}} : \mathrm{skew}(\underset{\sim}{\boldsymbol{A}}) = -\frac{1}{2}\underset{\approx}{\boldsymbol{\epsilon}} : \underset{\sim}{\boldsymbol{A}}\,, \tag{1}$$

and vice versa

$$\mathrm{skew}(\underset{\sim}{\boldsymbol{A}}) = -\underset{\approx}{\boldsymbol{\epsilon}} \cdot \overset{\times}{\underline{\boldsymbol{A}}}\,. \tag{2}$$

Double contraction is denoted $\underset{\sim}{\boldsymbol{A}} : \underset{\sim}{\boldsymbol{B}}$ and simple contraction is written as $\underline{\boldsymbol{b}} = \underset{\sim}{\boldsymbol{A}} \cdot \underline{\boldsymbol{a}}$. The scalar product of two vectors is $\underline{\boldsymbol{a}} \cdot \underline{\boldsymbol{b}} = \underline{\boldsymbol{a}}^T \underline{\boldsymbol{b}}$. On the other hand $\underset{\sim}{\boldsymbol{A}} = \underline{\boldsymbol{a}} \otimes \underline{\boldsymbol{b}}$ indicates the dyadic or tensor product of two vectors. The gradient of a vector is written as $\underline{\boldsymbol{a}} \otimes \nabla$ and the divergence of a vector or tensor is written as $\nabla \cdot \underline{\boldsymbol{a}}$ or $\underset{\sim}{\boldsymbol{A}} \cdot \nabla$, respectively (differentiation of a tensor is assumed to act on the second index). The curl operator is denoted $\nabla \times \underset{\sim}{\boldsymbol{A}}$. In the case a distinction is made between the deformed and reference configurations, differentiation with respect to the reference coordinates is denoted ∇_0.

2. Phase field approaches for grain boundary migration

There exist several mathematical approaches that deal with the dynamics of moving interfaces. One such approach is the phase field method. A phase field model of Allen-Cahn type [Allen and Cahn, 1979] considers a non-conserved order parameter ϕ (the phase field) which takes distinct values for each phase in the bulk and varies fast but continuously over interface regions. The free energy of the system associated with phase field is given by

$$\mathcal{F}_{PF} = \int_\Omega \psi_{PF}(\phi, \nabla\phi)\mathrm{d}\Omega = \int_\Omega \left[f(\phi) + \frac{a^2}{2}|\nabla\phi| \right] \mathrm{d}\Omega \,. \tag{3}$$

It is then postulated that the dynamics of the phase field can be found from the (vanishing) variational derivative of $\mathcal{F}_{PF}$ according to

$$\eta_\phi \, \dot{\phi} = -\frac{\delta\mathcal{F}}{\delta\phi} \,, \tag{4}$$

where η_ϕ is a viscosity type parameter that controls the time scale of relaxation towards equilibrium and thereby the mobility of the interface. The contribution $f(\phi)$ to the energy density essentially determines the composition of different phases in the bulk. For two separate phases, such as liquid or solid, $f(\phi)$ is in general a double well polynomial with one local minima for each of the two corresponding values of ϕ. The gradient term $\frac{a^2}{2}|\nabla\phi|$ represents the interface energy and localizes the grain boundaries to regions of width proportional to the parameter a.

In a solid polycrystal of a single phase material, grains are distinguished by their relative lattice orientations. The above standard model is not directly applicable to the problem of grain boundary migration in this case. Instead, extended approaches based on the general idea of the generic phase field model have been proposed. In the so-called multi-phase field method, the orientations are represented indirectly by assigning each orientation or grain an order parameter whereas in the orientation phase field approach, the crystal orientation itself is considered an order parameter. A brief outline of both methods will be given below. The discussion will focus on grain boundary migration in solid polycrystals, although both models have a wider scope of possible applications.

2.1. *Multi-phase field model*

Adopting the multi-phase field (MPF) approach [Steinbach *et al.*, 1996; Steinbach and Pezzolla, 1999], each crystal or rather crystal orientation can be represented by one of in total N non-conserved phase field variables ϕ_i, $i = 1, \ldots, N$. The ϕ_i are not independent as the sum of all fields at any one point is one, i.e. $\sum_i^N \phi_i = 1$. Each phase field furthermore takes the value one for a unique grain or orientation and is zero in all other grains. Several phases at once are present only at interfaces (two fields at a boundary between two grains, three fields at a triple junction and so on). The phase fields are not themselves the orientation but rather represent

the volume fraction of phase i, corresponding to a given orientation, present at a material point. The following equations govern a multi-phase field problem with N individual phases [Steinbach, 2009]. First, the energy is given by

$$\mathcal{F}_{MPF} = \int_{\Omega} \sum_{i=1}^{N} \frac{4\,\sigma_{ij}}{a} \left[-\frac{a^2}{\pi} \nabla\phi_i \cdot \nabla\phi_j + \phi_i\,\phi_j \right] \mathrm{d}\Omega\,. \tag{5}$$

Note that for $N = 2$ and $\phi_j = 1 - \phi_i$, the term $\phi_i\,\phi_j$ represents a double obstacle potential rather than a double well [Steinbach and Pezzolla, 1999]. The parameters σ_{ij} and a represent the interface energy between the phases and the interface width, respectively. Second, the evolution of the phase field ϕ_i can be found from

$$\dot{\phi}_i = -\sum_{j=1}^{N} \frac{\pi^2}{8\,a\,N} M_{ij} \left[\frac{\delta\mathcal{F}_{MPF}}{\delta\phi_i} - \frac{\delta\mathcal{F}_{MPF}}{\delta\phi_j}\,, \right] \tag{6}$$

where M_{ij} is the mobility of the interface.

It is possible to account for a large number N of phase fields and thus individual orientations, but the multi-phase field approach still has limitations when it comes to representing a real microstructure. In particular this is the case when viscoplastic deformations are taken into account as these may lead to considerable microstructural changes including heterogeneous lattice orientation developing even within grains. In the multi-phase field model grains are considered as having homogeneous orientation and reinitializing the grain structure would be necessary to take into account the formation of new subgrains due to deformation. It is not evident how a strongly coupled theory would deal with updating the orientation at individual material points due to concurrent viscoplastic deformation and grain boundary migration. The multi-phase field model has nevertheless been successful in sequentially coupled approaches [Takaki *et al.*, 2009; Takaki and Tomita, 2010; Güvenç *et al.*, 2013, 2014; Vondrous *et al.*, 2015] to model static or dynamic recrystallization.

2.2. *Orientation phase field model*

In the model by Kobayashi *et al.* [2000] and Warren *et al.* [2003] (which will be referred to hereafter as the KWC model), the basic phase field model is extended by considering also the crystal orientation to behave as a phase field, varying continuously over interfaces between grains and having its own relaxational dynamics. It is clear that this approach differs considerably from the multi-phase field model. First, only two fields are necessary to represent the crystal structure. For a pure solid, the field $\phi \in [0, 1]$ is considered a coarse grained order parameter which takes the value one in a perfect crystal and goes to zero in the grain boundaries. The KWC model was formulated in two dimensions, allowing the crystal orientation everywhere to be represented by the scalar field θ representing a rotation around the out-of-plane axis relative to a fixed frame. Second, this representation of the crystal orientation as a continuous field allows for heterogeneities to develop even

inside grains. This makes the KWC approach particularly well suited to couple with a viscoplastic continuum mechanics theory.

As the orientation is measured relative to some fixed frame, only its gradient enters the energy density. Kobayashi *et al.* [2000] showed that two terms are necessary to include, a linear term in $|\boldsymbol{\nabla}\theta|$ in order to energetically favor localized grain boundaries, and (at least) a higher order term $|\boldsymbol{\nabla}\theta|^2$ to smooth the profiles of η and θ to allow for the grain boundaries to be mobile. For small misorientations, $\nabla\theta$ is a measure of the lattice curvature. Later in this paper the relation between lattice curvature and dislocations will be elaborated and the connection to higher order crystal plasticity theories will be discussed.

The specific dimensionless (overbar indicates non-dimensionalized operators and parameters) KWC energy takes the form

$$\overline{\mathcal{F}}_{KWC} = \int_{\overline{\Omega}} \left[f(\phi) + \frac{\overline{a}^2}{2}|\overline{\nabla}\phi|^2 + \overline{s}\, g(\phi)|\overline{\nabla}\theta| + \frac{\overline{\varepsilon}^2}{2} h(\phi)|\overline{\nabla}\theta|^2 \right] \mathrm{d}\overline{\Omega}\,. \tag{7}$$

The functions $g(\phi)$ and $h(\phi)$ are required to be monotonically increasing with the variable ϕ. The function $f(\phi)$ has a single minimum at $\phi = 1$ (for the application of grain boundary migration in solids). Equilibrium is characterized by a vanishing variational derivative and it is postulated according to the standard phase field approach that relaxation is governed by rate equations of the following (dimensionless) form

$$Q\,\overline{\eta}_\phi\,\dot{\phi} = -\frac{\delta\overline{\mathcal{F}}_{KWC}}{\delta\phi} = \overline{a}^2\underline{\Delta}\phi - f_\phi - \overline{s}\, g_\phi|\overline{\nabla}\theta| - \frac{\overline{\varepsilon}^2}{2} h_\phi|\overline{\nabla}\theta|^2\,, \tag{8}$$

$$P\,\overline{\eta}_\theta\,\phi^2\,\dot{\theta} = -\frac{\delta\overline{\mathcal{F}}_{KWC}}{\delta\theta} = \overline{\nabla}\cdot\left[\overline{\varepsilon}^2 h\overline{\nabla}\theta + \overline{s}\, g\frac{\overline{\nabla}\theta}{|\overline{\nabla}\theta|}\right]. \tag{9}$$

In the above equations, Q and P are mobility functions which, in general, can depend on the state variables such that $Q = Q(\phi, \nabla\phi, \nabla\theta; T)$ and $P = P(\phi, \nabla\phi, \nabla\theta; T)$ with T being the temperature. The presence of the linear term $|\overline{\nabla}\theta|$ results in an infinite diffusion type of equation for the evolution of the field θ which requires some numerical regularization [Kobayashi and Giga, 1999]. Due to the coupling functions, both fields will have interfaces at the same locations but the width of the interface region will in general be smaller for θ than for ϕ [Lobkovsky and Warren, 2001].

3. Crystal plasticity and dislocation densities

This section gives a brief overview of classic crystal plasticity theory. The link between the plasticity theory and dislocation densities is elaborated. Two types of dislocations were identified by Ashby [1970]: so–called statistically stored dislocations (SSDs) which are accumulated within grains during viscoplastic deformation due to random trapping, and geometrically necessary dislocations (GNDs) which are associated with incompatible deformations and can be expressed in terms of plastic strain gradients and lattice curvature.

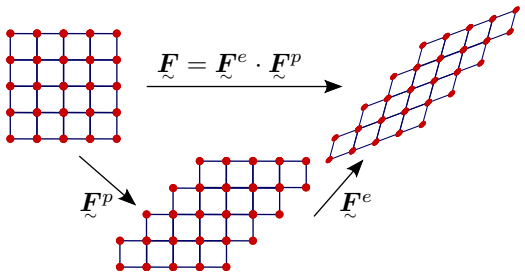

Fig. 1. In the isoclinic intermediate configuration the lattice directors retain their orientation with respect to the undeformed configuration.

3.1. *Kinematics of single crystal plasticity*

Let $\underline{\boldsymbol{X}}$ be the position of a material point in an undeformed body $\mathcal{B}_0$ and $\underline{\boldsymbol{x}}$ its position in the current, deformed state $\mathcal{B}_t$. The deformation gradient tensor $\underset{\sim}{\boldsymbol{F}} = \underline{\boldsymbol{\varphi}} \otimes \nabla_0$ is the material gradient of the map $\underline{\boldsymbol{x}} = \underline{\boldsymbol{\varphi}}(\underline{\boldsymbol{X}}, t)$ which describes the motion of material points between the reference and deformed configurations. Its determinant $J = \det \underset{\sim}{\boldsymbol{F}} > 0$ describes the volume change due to the deformation. With the displacement vector given by $\underline{\boldsymbol{u}} = \underline{\boldsymbol{x}} - \underline{\boldsymbol{X}}$, the deformation gradient can be written as

$$\underset{\sim}{\boldsymbol{F}} = \underset{\sim}{\boldsymbol{I}} + \underline{\boldsymbol{u}} \otimes \nabla_0 = \underset{\sim}{\boldsymbol{I}} + \underset{\sim}{\boldsymbol{H}} \,. \tag{10}$$

Since $\underset{\sim}{\boldsymbol{F}}$ is invertible with positive determinant, it is always possible to separate the deformation into a proper orthogonal rotation $\underset{\sim}{\boldsymbol{R}}$ and a pure stretch $\underset{\sim}{\boldsymbol{U}}$ or $\underset{\sim}{\boldsymbol{V}}$ such that $\underset{\sim}{\boldsymbol{F}} = \underset{\sim}{\boldsymbol{R}} \cdot \underset{\sim}{\boldsymbol{U}} = \underset{\sim}{\boldsymbol{V}} \cdot \underset{\sim}{\boldsymbol{R}}$.

In plasticity, a multiplicative split $\underset{\sim}{\boldsymbol{F}} = \underset{\sim}{\boldsymbol{F}}^e \cdot \underset{\sim}{\boldsymbol{F}}^p$ is generally adopted [Kröner, 1959; Lee, 1969] whereby a fictitious, stress-free intermediate configuration is introduced. It is important to note that whereas $\underset{\sim}{\boldsymbol{F}}$ is compatible (i.e. its curl is zero), this is in general not the case for the elastic or plastic deformations. Furthermore, the intermediate configuration is not unique as any rigid rotation of the body will result in another stress-free configuration. Some choice therefore has to be made to ensure the uniqueness of the multiplicative decomposition. In crystal plasticity it is convenient to adopt an isoclinic intermediate configuration [Mandel, 1972, 1973] based on the observation that plastic deformation takes place by dislocation slip processes that leave the orientation of the lattice vectors intact compared to the reference state. This is demonstrated schematically in figure 1. There is thus a clear distinction between lattice directions on the one hand and material lines on the other, since lattice directions are not necessarily made up of the same points in the reference and deformed configurations and the glide of dislocations during plastic deformation does not distort the lattice although it may shear material lines.

The (spatial) velocity gradient can be expressed in terms of the deformation gradient tensor according to

$$\underset{\sim}{\boldsymbol{L}} = \underline{\boldsymbol{v}} \otimes \nabla = \dot{\underset{\sim}{\boldsymbol{F}}} \cdot \underset{\sim}{\boldsymbol{F}}^{-1} = \operatorname{sym}(\underset{\sim}{\boldsymbol{L}}) + \operatorname{skew}(\underset{\sim}{\boldsymbol{L}}) = \underset{\sim}{\boldsymbol{D}} + \underset{\sim}{\boldsymbol{W}} \,, \tag{11}$$

where $\underset{\sim}{\boldsymbol{D}}$ and $\underset{\sim}{\boldsymbol{W}}$ are the strain rate and spin tensors, respectively. In terms of the elastic and plastic contributions, the velocity gradient tensor can be written as

$$\underset{\sim}{\boldsymbol{L}} = \dot{\underset{\sim}{\boldsymbol{F}}} \cdot \underset{\sim}{\boldsymbol{F}}^{-1} = \dot{\underset{\sim}{\boldsymbol{F}}}^{e} \cdot \underset{\sim}{\boldsymbol{F}}^{e-1} + \underset{\sim}{\boldsymbol{F}}^{e} \cdot \dot{\underset{\sim}{\boldsymbol{F}}}^{p} \cdot \underset{\sim}{\boldsymbol{F}}^{p-1} \cdot \underset{\sim}{\boldsymbol{F}}^{e-1} = \underset{\sim}{\boldsymbol{L}}^{e} + \underset{\sim}{\boldsymbol{L}}^{p} \,. \tag{12}$$

The evolution of plastic deformation by slip on N possible slip systems can be described in the intermediate configuration by

$$\dot{\underset{\sim}{\boldsymbol{F}}}^{p} \cdot \underset{\sim}{\boldsymbol{F}}^{p-1} = \sum_{\alpha=1}^{N} \dot{\gamma}^{\alpha} \underline{\boldsymbol{\ell}}^{\alpha} \otimes \underline{\boldsymbol{n}}^{\alpha} \,, \tag{13}$$

where $\underline{\boldsymbol{\ell}}^{\alpha}$ and $\underline{\boldsymbol{n}}^{\alpha}$ are the slip direction and slip plane normal and $\dot{\gamma}^{\alpha}$ is the slip rate which must be specified. Typically, for each load situation, $\dot{\gamma}^{\alpha}$ is non-zero only for a sub-set of preferred slip systems.

The corresponding deformation measures and rates for small strains and small rotations can be found from linearization of the deformation gradient and its elastic and plastic contributions. It follows from

$$\underset{\sim}{\boldsymbol{F}}^{e} = \underset{\sim}{\boldsymbol{R}}^{e} \cdot \underset{\sim}{\boldsymbol{U}}^{e} \approx \left[\underset{\sim}{\boldsymbol{I}} + \underset{\sim}{\boldsymbol{\vartheta}}^{e} \right] \cdot \left[\underset{\sim}{\boldsymbol{I}} + \underset{\sim}{\boldsymbol{\varepsilon}}^{e} \right] \approx \underset{\sim}{\boldsymbol{I}} + \underset{\sim}{\boldsymbol{\varepsilon}}^{e} + \underset{\sim}{\boldsymbol{\vartheta}}^{e} = \underset{\sim}{\boldsymbol{I}} + \underset{\sim}{\boldsymbol{H}}^{e} \,, \tag{14}$$

$$\underset{\sim}{\boldsymbol{F}}^{p} = \underset{\sim}{\boldsymbol{R}}^{p} \cdot \underset{\sim}{\boldsymbol{U}}^{p} \approx \left[\underset{\sim}{\boldsymbol{I}} + \underset{\sim}{\boldsymbol{\vartheta}}^{p} \right] \cdot \left[\underset{\sim}{\boldsymbol{I}} + \underset{\sim}{\boldsymbol{\varepsilon}}^{p} \right] \approx \underset{\sim}{\boldsymbol{I}} + \underset{\sim}{\boldsymbol{\varepsilon}}^{p} + \underset{\sim}{\boldsymbol{\vartheta}}^{p} = \underset{\sim}{\boldsymbol{I}} + \underset{\sim}{\boldsymbol{H}}^{p} \tag{15}$$

that

$$\underset{\sim}{\boldsymbol{F}} = \underset{\sim}{\boldsymbol{I}} + \underset{\sim}{\boldsymbol{H}} \approx \underset{\sim}{\boldsymbol{I}} + \underset{\sim}{\boldsymbol{H}}^{e} + \underset{\sim}{\boldsymbol{H}}^{p} = \underset{\sim}{\boldsymbol{I}} + \underset{\sim}{\boldsymbol{\varepsilon}} + \underset{\sim}{\boldsymbol{\vartheta}} \,, \tag{16}$$

where $\underset{\sim}{\boldsymbol{\varepsilon}} = \underset{\sim}{\boldsymbol{\varepsilon}}^{e} + \underset{\sim}{\boldsymbol{\varepsilon}}^{p}$ is the symmetric small strain tensor and $\underset{\sim}{\boldsymbol{\vartheta}} = \underset{\sim}{\boldsymbol{\vartheta}}^{e} + \underset{\sim}{\boldsymbol{\vartheta}}^{p}$ is skew-symmetric and represents small rotations. The linearized total and plastic rate of deformation and spin tensors become

$$\underset{\sim}{\boldsymbol{D}} \approx \dot{\underset{\sim}{\boldsymbol{\varepsilon}}} \,, \tag{17}$$

$$\underset{\sim}{\boldsymbol{W}} \approx \underset{\sim}{\boldsymbol{\omega}} = \dot{\underset{\sim}{\boldsymbol{\vartheta}}} \,, \tag{18}$$

$$\underset{\sim}{\boldsymbol{D}}^{p} = \mathrm{sym}(\underset{\sim}{\boldsymbol{L}}^{\mathrm{p}}) \approx \dot{\underset{\sim}{\boldsymbol{\varepsilon}}}^{\mathrm{p}} = \mathrm{sym} \left(\sum_{\alpha=1}^{\mathrm{N}} \dot{\gamma}^{\alpha} \underline{\boldsymbol{\ell}}^{\alpha} \otimes \underline{\boldsymbol{n}}^{\alpha} \right) \,, \tag{19}$$

$$\underset{\sim}{\boldsymbol{W}}^{p} = \mathrm{skew}(\underset{\sim}{\boldsymbol{L}}^{\mathrm{p}}) \approx \underset{\sim}{\boldsymbol{\omega}}^{\mathrm{p}} = \dot{\underset{\sim}{\boldsymbol{\vartheta}}}^{\mathrm{p}} = \mathrm{skew} \left(\sum_{\alpha=1}^{\mathrm{N}} \dot{\gamma}^{\alpha} \underline{\boldsymbol{\ell}}^{\alpha} \otimes \underline{\boldsymbol{n}}^{\alpha} \right) \,. \tag{20}$$

The elastic contributions follow from the additive decompositions, i.e. $\dot{\underset{\sim}{\boldsymbol{\varepsilon}}}^{e} = \dot{\underset{\sim}{\boldsymbol{\varepsilon}}} - \dot{\underset{\sim}{\boldsymbol{\varepsilon}}}^{p}$ and $\underset{\sim}{\boldsymbol{\omega}}^{e} = \dot{\underset{\sim}{\boldsymbol{\vartheta}}}^{e} = \underset{\sim}{\boldsymbol{\omega}} - \underset{\sim}{\boldsymbol{\omega}}^{p}$.

3.2. *Lattice curvature and the dislocation density tensor*

The elastic and plastic parts of $\underset{\sim}{\boldsymbol{F}}$ are in general not compatible (they are not the gradients of a vector field). A closed circuit C in $\mathcal{B}_0$ is therefore in general mapped onto an open circuit in the intermediate configuration by $\underset{\sim}{\boldsymbol{F}}^{p}$, and this is likewise true for the inverse mapping of a closed circuit c in $\mathcal{B}_t$ by $\underset{\sim}{\boldsymbol{F}}^{e-1}$. In the continuum

description, the true Burgers vector for a smooth, oriented surface s in $\mathcal{B}_t$, with boundary c and containing $\underline{\mathrm{d}\boldsymbol{x}}$, can then be defined from the closure failure as

$$\underline{\boldsymbol{b}} = \int_c \underset{\sim}{\boldsymbol{F}}^{e-1} \cdot \underline{\mathrm{d}\boldsymbol{x}} = -\int_s \left[\nabla \times \underset{\sim}{\boldsymbol{F}}^{e-1} \right] \cdot \underline{\mathrm{d}\boldsymbol{s}} = \int_s \underset{\sim}{\boldsymbol{\alpha}} \cdot \underline{\mathrm{d}\boldsymbol{s}} \,, \tag{21}$$

where $\underline{\boldsymbol{n}}$ is the outward normal and $\underset{\sim}{\boldsymbol{\alpha}}$ is the dislocation density tensor which can thus be defined as

$$\underset{\sim}{\boldsymbol{\alpha}} \equiv -\nabla \times \underset{\sim}{\boldsymbol{F}}^{e-1} \,. \tag{22}$$

An alternative definition of the dislocation density tensor can be found by pull-back and push-forward operations such that

$$\begin{aligned} \int_s \underset{\sim}{\boldsymbol{\alpha}} \cdot \underline{\mathrm{d}\boldsymbol{s}} &= \int_c \underset{\sim}{\boldsymbol{F}}^{e-1} \cdot \underline{\mathrm{d}\boldsymbol{x}} = \int_C \underset{\sim}{\boldsymbol{F}}^{e-1} \cdot \underset{\sim}{\boldsymbol{F}} \cdot \underline{\mathrm{d}\boldsymbol{X}} = \int_C \underset{\sim}{\boldsymbol{F}}^{p} \cdot \underline{\mathrm{d}\boldsymbol{X}} \\ &= -\int_S \left[\nabla_0 \times \underset{\sim}{\boldsymbol{F}}^{p} \right] \cdot \underline{\mathrm{d}\boldsymbol{S}} = -\int_s \frac{1}{J} \left[\nabla_0 \times \underset{\sim}{\boldsymbol{F}}^{p} \right] \cdot \underset{\sim}{\boldsymbol{F}}^{T} \cdot \underline{\mathrm{d}\boldsymbol{s}} \end{aligned} \,, \tag{23}$$

where Nanson's formula was used to relate the surface elements $\underline{\mathrm{d}\boldsymbol{s}}$ in $\mathcal{B}_t$ and $\underline{\mathrm{d}\boldsymbol{S}}$ in $\mathcal{B}_0$. This gives an alternative format for the dislocation density tensor in terms of the plastic deformation, with

$$\underset{\sim}{\boldsymbol{\alpha}} \equiv -\frac{1}{J} \left[\nabla_0 \times \underset{\sim}{\boldsymbol{F}}^{p} \right] \cdot \underset{\sim}{\boldsymbol{F}}^{T} \,. \tag{24}$$

For small deformations, with

$$\underset{\sim}{\boldsymbol{F}}^{e-1} \approx \underset{\sim}{\boldsymbol{I}} - \underset{\sim}{\boldsymbol{H}}^{e} \,, \tag{25}$$

the dislocation density tensor becomes

$$\underset{\sim}{\boldsymbol{\alpha}} \approx \nabla \times \underset{\sim}{\boldsymbol{H}}^{e} = -\nabla \times \underset{\sim}{\boldsymbol{H}}^{p} \,, \tag{26}$$

where the latter equality follows from the compatibility of the total deformation gradient.

If the elastic stretches are small[a], which can be expected for metals, the dislocation density tensor can be approximated as

$$\underset{\sim}{\boldsymbol{\alpha}} = -\nabla \times \underset{\sim}{\boldsymbol{F}}^{e-1} \approx -\nabla \times \underset{\sim}{\boldsymbol{R}}^{eT} \,, \tag{27}$$

furthermore if the elastic rotations are also small then

$$\underset{\sim}{\boldsymbol{\alpha}} \approx -\nabla \times \underset{\sim}{\boldsymbol{R}}^{eT} \approx -\nabla \times \left[\underset{\sim}{\boldsymbol{I}} - \underset{\sim}{\boldsymbol{\vartheta}}^{e} \right] = \nabla \times \underset{\sim}{\boldsymbol{\vartheta}}^{e} \,. \tag{28}$$

For small deformations the lattice curvature is given by the gradient of the pseudo-vector of the elastic rotation, i.e.

$$\underset{\sim}{\boldsymbol{\kappa}} \equiv \overset{\times}{\underline{\boldsymbol{\vartheta}}}^{e} \otimes \nabla \,. \tag{29}$$

[a]and in fact, if the elastic strain gradient also is small enough

From equations (28) and (29) follows the Nye relation [Nye, 1953]

$$\underset{\sim}{\boldsymbol{\alpha}} = \underset{\sim}{\boldsymbol{\kappa}}^{T} - \mathrm{tr}(\underset{\sim}{\boldsymbol{\kappa}})\,\underset{\sim}{\boldsymbol{I}}\,, \qquad \underset{\sim}{\boldsymbol{\kappa}} = \underset{\sim}{\boldsymbol{\alpha}}^{\mathrm{T}} - \frac{1}{2}\mathrm{tr}(\underset{\sim}{\boldsymbol{\alpha}})\,\underset{\sim}{\boldsymbol{I}}\,. \tag{30}$$

GND development due to local deformation incompatibility results in size-dependent material behavior. Higher order continuum crystal plasticity models which can take into consideration the effect of the dislocation density tensor are needed in this case, such as plastic strain gradient models [Fleck and Hutchinson, 1997] or Cosserat crystal plasticity [Forest *et al.*, 1997, 2001; Mayeur and McDowell, 2014]. The latter approach is used in this work and will be presented in the next section.

It appears that the lattice curvature tensor can be seen as an approximation of the full dislocation density tensor. Free energy potentials involving the norm and the square of the norm of the GND tensor were considered by Forest and Guéninchault [2013]; Wulfinghoff *et al.* [2015] in order to describe size effects in gradient crystal plasticity. They are closely related to the rank one and rank two lattice curvature potentials used in the KWC model. Relations between strain gradient, Cosserat and micromorphic crystal plasticity were established in [Forest, 2008; Cordero *et al.*, 2012].

3.3. *Dislocations and work hardening*

As the dislocation density increases (both GND and SSD), additional plastic glide becomes more difficult and the material hardens. This can be taken into consideration by assuming that the critically resolved shear stress τ_c^α (the critical value of the stress projected on slip system α for which plasticity occurs) is proportional to the scalar dislocation density ρ according to [Taylor, 1934; Franciosi *et al.*, 1980]

$$\tau_c^\alpha = \chi\,\mu\,b\sqrt{\sum_{\beta=1}^{N} h^{\alpha\beta}\,\rho^\beta}\,, \tag{31}$$

where N is the number of slip systems, μ is the shear modulus, b is the norm of the Burgers vector of the considered slip system family and χ is a proportionality factor close to 0.3 [Ashby, 1970]. The interaction matrix $h^{\alpha\beta}$ accounts for the anisotropic interaction between slip systems.

The evolution of dislocation content on slip system α can be described by competing mechanisms of multiplication and annihilation according to Kocks and Mecking [2003] and Teodosiu and Sidoroff [1976] as

$$\dot\rho^\alpha = \frac{1}{b}\left(K\sqrt{\sum_\beta \rho^\beta} - 2d\rho^\alpha\right)|\dot\gamma^\alpha|\,, \tag{32}$$

where the parameter K is a dislocation mobility constant and d is the critical annihilation distance between opposite sign dislocations.

Energy stored during viscoplastic deformation is also one of the most significant driving forces for grain boundary migration [Humphreys and Hatherly, 2004; Gottstein and Shvindlerman, 2010]. The stored energy and thereby driving pressure due to a dislocation density ρ can be expressed approximately as

$$\psi_\rho \approx \frac{1}{2}\mu\, b^2\, \rho\,. \tag{33}$$

Gottstein and Shvindlerman [2010] gives typical values of the driving pressure due to stored dislocations that are several magnitudes larger than the driving pressures due to grain boundary energy.

4. The coupled Cosserat–phase field theory

This section is dedicated to an overview of the coupled Cosserat–phase field model proposed by Ask *et al.* [2018b] with some modifications that are detailed below. The model is valid for the case of small strains, small rotations and small curvatures. The model can be formulated within the large deformation framework, as proposed in [Ask *et al.*, 2018a].

4.1. *Kinematics, deformation measures and balance laws*

The Cosserat rotation tensor $\underset{\sim}{\mathfrak{R}}$ describes the rotation of a triad of directors attached to each material point from the initial to the deformed state. This rotation is, a priori, independent of the displacements so that six degrees of freedom are necessary to describe the motion of the material point: the displacement vector $\underline{\boldsymbol{u}}$ and the microrotation pseudo-vector $\underline{\boldsymbol{\Theta}}$. In the small deformation setting the Cosserat rotation tensor is then given by

$$\underset{\sim}{\mathfrak{R}} = \underset{\sim}{\boldsymbol{I}} - \underset{\sim}{\boldsymbol{\epsilon}} \cdot \underline{\boldsymbol{\Theta}}\,, \tag{34}$$

and the linearized deformation measures are given by [Eringen and Kafadar, 1976; Forest *et al.*, 1997]

$$\underset{\sim}{\boldsymbol{e}} = \underline{\boldsymbol{u}} \otimes \nabla + \underset{\sim}{\boldsymbol{\epsilon}} \cdot \underline{\boldsymbol{\Theta}}\,, \qquad \underset{\sim}{\boldsymbol{\kappa}} = \underline{\boldsymbol{\Theta}} \otimes \nabla\,. \tag{35}$$

In the small strain setting the decomposition of the deformation into elastic and plastic contributions is additive and given by

$$\underset{\sim}{\boldsymbol{e}} = \underset{\sim}{\boldsymbol{e}}^e + \underset{\sim}{\boldsymbol{e}}^p\,. \tag{36}$$

For simplicity, an elasto-plastic decomposition of the curvature tensor will not be pursued here, although possible following [Forest and Sievert, 2003]. Ask *et al.* [2018b] introduced a third contribution in the decomposition of $\underset{\sim}{\boldsymbol{e}}$ in the form of a skew-symmetric eigendeformation with its own evolution equation. Here, a modified evolution law for the plastic deformation will be considered instead. The two approaches lead to formally identical governing equations.

By simple inspection, it is evident that the symmetric part of the Cosserat deformation is the usual small strain tensor, i.e.

$$\operatorname{sym}(\underset{\sim}{\boldsymbol{e}}) = \underset{\sim}{\boldsymbol{\varepsilon}}\,, \tag{37}$$

whereas the skew-symmetric part is

$$\operatorname{skew}(\underset{\sim}{\boldsymbol{e}}) = \underset{\sim}{\boldsymbol{\vartheta}} + \underset{\sim}{\underset{\sim}{\boldsymbol{\epsilon}}} \cdot \underline{\boldsymbol{\Theta}}\,. \tag{38}$$

Its rate can be written as

$$\dot{\underset{\sim}{\boldsymbol{e}}} = \dot{\underset{\sim}{\boldsymbol{\varepsilon}}} + \underset{\sim}{\boldsymbol{\omega}} + \underset{\sim}{\underset{\sim}{\boldsymbol{\epsilon}}} \cdot \dot{\underline{\boldsymbol{\Theta}}}\,, \tag{39}$$

with the skew-symmetric part represented by a pseudo-vector

$$\dot{\overset{\times}{\underline{\boldsymbol{e}}}} = \overset{\times}{\underline{\boldsymbol{\omega}}} - \dot{\underline{\boldsymbol{\Theta}}}\,. \tag{40}$$

This latter expression relates the relative rotation of the material and the motion of the microstructural directors that is described by the Cosserat rotation. In particular, taking into account plasticity and introducing the elastic and plastic spin pseudo-vectors $\overset{\times}{\underline{\boldsymbol{\omega}}}^{\,p} := \dot{\overset{\times}{\underline{\boldsymbol{e}}}}^{\,p}$ and $\overset{\times}{\underline{\boldsymbol{\omega}}}^{\,e} := \overset{\times}{\underline{\boldsymbol{\omega}}} - \overset{\times}{\underline{\boldsymbol{\omega}}}^{\,p}$, respectively, the rate of the skew-symmetric deformation can be expressed as

$$\overset{\times}{\underline{\boldsymbol{\omega}}}^{\,e} - \dot{\underline{\boldsymbol{\Theta}}} = \dot{\overset{\times}{\underline{\boldsymbol{e}}}}^{\,e}\,. \tag{41}$$

The above expression provides a link between the lattice and microrotation rates that enables a formulation where the Cosserat directors remain parallel to the lattice vectors as the body deforms. This is achieved by enforcement of the internal constraint

$$\overset{\times}{\underline{\boldsymbol{e}}}^{\,e} \equiv 0. \tag{42}$$

either on the constitutive level [Forest *et al.*, 1997, 2000; Mayeur *et al.*, 2011; Mayeur and McDowell, 2014; Blesgen, 2014] or directly using Lagrange multipliers.

Finally, in order to account for migrating grain boundaries the Cosserat theory is enhanced with a phase field variable $\phi \in [0, 1]$ which is interpreted in this context as a coarse-grained measure of crystalline order. In the bulk of an undeformed grain the order parameter takes the value $\phi = 1$ whereas $\phi < 1$ in grain boundaries or even inside plastically deformed grains due to build-up of so called statistically stored dislocations.

The balance equations and corresponding boundary conditions for the coupled formulation are found by applying the method of virtual power on the set of virtual field variables

$$\mathcal{V} = \{\dot{\phi}, \nabla\dot{\phi}, \dot{\underline{\boldsymbol{u}}}, \dot{\underline{\boldsymbol{u}}} \otimes \nabla, \dot{\underline{\boldsymbol{\Theta}}}, \dot{\underline{\boldsymbol{\Theta}}} \otimes \nabla\}\,, \tag{43}$$

and their associated generalized stresses [Ask *et al.*, 2018b; Abrivard *et al.*, 2012a; Ammar *et al.*, 2009]. By adopting the formalism of Gurtin [1996]; Gurtin and Lusk [1999] for the phase field, the integration of the phase field equations in the overall

approach is straightforward. The resulting field and boundary equations are given by

$$\nabla \cdot \underline{\boldsymbol{\xi}}_{\phi} + \pi_{\phi} + \pi_{\phi}^{\text{ext}} = 0 \qquad \text{in } \Omega\,, \tag{44}$$

$$\underset{\sim}{\boldsymbol{\sigma}} \cdot \nabla + \underline{\boldsymbol{f}}^{\text{ext}} = \underline{\mathbf{0}} \qquad \text{in } \Omega\,, \tag{45}$$

$$\underset{\sim}{\boldsymbol{m}} \cdot \nabla + 2\,\overset{\times}{\underset{\sim}{\boldsymbol{\sigma}}} + \underline{\boldsymbol{c}}^{\text{ext}} = \underline{\mathbf{0}} \qquad \text{in } \Omega\,, \tag{46}$$

$$\underline{\boldsymbol{\xi}}_{\phi} \cdot \underline{\boldsymbol{n}} = \pi_{\phi}^{c} \qquad \text{on } \partial\Omega\,, \tag{47}$$

$$\underset{\sim}{\boldsymbol{\sigma}} \cdot \underline{\boldsymbol{n}} = \underline{\boldsymbol{f}}^{c} \qquad \text{on } \partial\Omega\,, \tag{48}$$

$$\underset{\sim}{\boldsymbol{m}} \cdot \underline{\boldsymbol{n}} = \underline{\boldsymbol{c}}^{c} \qquad \text{on } \partial\Omega\,. \tag{49}$$

The stress $\underset{\sim}{\boldsymbol{\sigma}}$ associated with the Cosserat deformation $\underset{\sim}{\boldsymbol{e}}$ is not the usual Cauchy stress and contains a skew-symmetric contribution that also appears in the balance equation for the couple stress $\underset{\sim}{\boldsymbol{m}}$ which is work conjugate to the curvature/wryness tensor $\underset{\sim}{\boldsymbol{\kappa}}$. The microstresses π_{ϕ} and $\underline{\boldsymbol{\xi}}_{\phi}$ in (44) are associated with the phase field ϕ and its gradient $\nabla\phi$, respectively. External body forces and couples are denoted by superscript $\langle\bullet\rangle^{\text{ext}}$ and contact forces and couples by superscript $\langle\bullet\rangle^{c}$, with $\underline{\boldsymbol{n}}$ the outward normal to the boundary $\partial\Omega$ of the body Ω.

4.2. *Constitutive and evolution equations*

The general constitutive equations used in this work comply with the thermodynamic principles [Ask *et al.*, 2018b]. In order to recover the phase field dynamics is is assumed that the stress π_{ϕ} contains energetic and dissipative contributions so that

$$\pi_{\phi} = \pi_{\phi}^{eq} + \pi_{\phi}^{neq}\,. \tag{50}$$

The following expressions are proposed for the energetic quantities

$$\pi_{\phi}^{eq} = -\frac{\partial \psi}{\partial \phi}\,, \tag{51}$$

$$\underline{\boldsymbol{\xi}}_{\phi} = \frac{\partial \psi}{\partial \nabla \phi}\,, \tag{52}$$

$$\underset{\sim}{\boldsymbol{\sigma}} = \frac{\partial \psi}{\partial \underset{\sim}{\boldsymbol{e}}^{e}}\,, \tag{53}$$

$$\underset{\sim}{\boldsymbol{m}} = \frac{\partial \psi}{\partial \underset{\sim}{\boldsymbol{\kappa}}}\,, \tag{54}$$

assuming that

$$\rho\,\Psi = \psi(\phi, \nabla\phi, \underset{\sim}{\boldsymbol{e}}^{e}, \underset{\sim}{\boldsymbol{\kappa}}, r^{\alpha})\,, \tag{55}$$

where Ψ is the Helmholtz energy density and r^{α} are internal variables related to the inelastic behavior. For the dissipative processes it is assumed that there exists a dissipation potential

$$\Omega = \Omega^{p}(\underset{\sim}{\boldsymbol{\sigma}}) + \Omega^{\alpha}(R^{\alpha}) + \Omega^{\phi}(\pi_{\phi}^{neq})\,, \tag{56}$$

where

$$R^\alpha = \frac{\partial \psi}{\partial r^\alpha} \tag{57}$$

are thermodynamic forces associated with r^α and evolution equations, including the flow and hardening rules, are derived from the dissipation potential

$$\dot{\underset{\sim}{\boldsymbol{e}}}^p = \frac{\partial \Omega^p}{\partial \underset{\sim}{\boldsymbol{\sigma}}}, \quad \dot{r}^\alpha = -\frac{\partial \Omega^\alpha}{\partial R^\alpha}, \quad \dot{\phi} = -\frac{\partial \Omega^\phi}{\partial \pi_\phi^{neq}}. \tag{58}$$

The potential Ω chosen in the following fulfills convexity conditions which ensure positive dissipation. The formulation presented here differs somewhat from the one presented in [Ask *et al.*, 2018b] in that there are fewer contributions to the dissipation potential. This is for two reasons. First, a dissipative contribution to the stress $\underset{\sim}{\boldsymbol{\sigma}}$ was considered in the previous work which led to a separate evolution law for the relative rotation in the spirit of the KWC model. This contribution is necessary in the KWC model but superfluous in the coupled approach and therefore not considered here. Second, the separate eigendeformation type tensor introduced in [Ask *et al.*, 2018b] is considered as a part of the plastic deformation in this work and its evolution is derived from Ω^p.

4.3. *Coupled model*

The free energy density for the coupled problem is given by Ask *et al.* [2018b]

$$\begin{aligned}\psi(\phi, \nabla\phi, \underset{\sim}{\boldsymbol{e}}^e, \underset{\sim}{\boldsymbol{\kappa}}, r^\alpha) = f_0 \left[f(\phi) + \frac{a^2}{2}|\nabla\phi|^2 + s\, g(\phi)||\underset{\sim}{\boldsymbol{\kappa}}|| + \frac{\varepsilon^2}{2} h(\phi)||\underset{\sim}{\boldsymbol{\kappa}}||^2 \right] \\ + \frac{1}{2}\underset{\sim}{\boldsymbol{\varepsilon}}^e : \underset{\approx}{\boldsymbol{E}}^s : \underset{\sim}{\boldsymbol{\varepsilon}}^e + 2\,\mu_c\, \underline{\overset{\times}{\boldsymbol{e}}}^{\,e} \cdot \underline{\overset{\times}{\boldsymbol{e}}}^{\,e} + \psi_\rho(\phi, r^\alpha)\,.\end{aligned} \tag{59}$$

The first line can be considered a generalization to three dimensions of the KWC energy (7). It contains a grain boundary term due to the phase field ϕ and a contribution due to the lattice curvature tensor $\underset{\sim}{\boldsymbol{\kappa}}$. The coupling functions $g(\phi)$ and $h(\phi)$ are required to be non-negative and to increase monotonously with ϕ. The parameter f_0 has dimension [Pa] and a, s and ε have dimension [m]. While the main motivation for including the linear term corresponding to $||\nabla\underset{\sim}{\boldsymbol{\kappa}}||$ in the KWC model was to localize the grain boundaries, the relationship between the lattice curvature and the GND tensor allows for a physical interpretation where the linear term represents the self energy of the GNDs and the quadratic term is an interaction energy [Ohno and Okumura, 2007; Mesarovic *et al.*, 2015; Wulfinghoff *et al.*, 2015]. The link between the KWC model and a higher order crystal plasticity theory was also recognized in the work of Admal *et al.* [2018], who formulated a similar coupled approach using the full GND tensor.

The second line in (59) contains the energy contribution due to symmetric and skew-symmetric elastic deformation. A standard quadratic form is adopted for the symmetric strain with the (possibly anisotropic) elasticity tensor $\underset{\approx}{\boldsymbol{E}}^s$. By choosing

the Cosserat parameter μ_c to be large enough, the skew-symmetric part of the deformation is penalized and the Cosserat microrotation is required to follow the lattice orientation, thus approaching the constraint (42). The following state laws are obtained

$$\mathrm{sym}(\underset{\sim}{\boldsymbol{\sigma}}) = \underset{\approx}{\boldsymbol{E}}^s : \underset{\sim}{\boldsymbol{\varepsilon}}\,, \tag{60}$$

$$\overset{\times}{\underline{\boldsymbol{\sigma}}} = 2\,\mu_c \overset{\times}{\underline{\boldsymbol{e}}}^e \tag{61}$$

$$\underset{\sim}{\boldsymbol{m}} = f_0 \left[s\, g(\phi) \frac{1}{||\underset{\sim}{\boldsymbol{\kappa}}||} + \varepsilon^2\, h(\phi) \right] \underset{\sim}{\boldsymbol{\kappa}}\,, \tag{62}$$

$$\pi_\phi^{eq} = -\, f_0 \left[1 - \phi - s\, \frac{\partial g}{\partial \phi} ||\underset{\sim}{\boldsymbol{\kappa}}|| - \frac{\varepsilon^2}{2} \frac{\partial h}{\partial \phi} ||\underset{\sim}{\boldsymbol{\kappa}}||^2 \right] - \sum_{\alpha=1}^{N} \frac{\chi}{2}\, \mu\, r^{\alpha 2}\,, \tag{63}$$

$$\underline{\boldsymbol{\xi}}_\phi = f_0\, a^2 \nabla \phi\,. \tag{64}$$

The very last term in (59) is the stored energy due to accumulated dislocations. It is taken to be

$$\psi_\rho(\phi, r^\alpha) = \phi \sum_{\alpha=1}^{N} \frac{\chi}{2}\, \mu\, r^{\alpha 2}\,. \tag{65}$$

where N is the number of slip systems and r^α are internal variables. Note that there is a coupling with the phase field variable ϕ. This coupling ensures that the stored energy acts as a driving force for grain boundary migration. The internal variables are assumed to be related to the scalar dislocation densities via

$$r^\alpha = b \sqrt{\sum_{\beta=1}^{N} h^{\alpha\beta} \rho^\beta}\,. \tag{66}$$

This leads to the following Taylor hardening expression

$$R^\alpha = \frac{\partial \psi}{\partial r^\alpha} = \phi\, \chi\, \mu\, r^\alpha = \phi\, \chi\, \mu\, b \sqrt{\sum_{\beta=1}^{N} h^{\alpha\beta} \rho^\beta}\,. \tag{67}$$

for the thermodynamic force R^α which is now interpreted as the critical resolved shear stress on slip system α.

The plastic dissipation potential Ω^p is assumed to be given by

$$\Omega^p = \sum_{\alpha=1}^{N} \frac{K_v}{n+1} \left\langle \frac{|\tau^\alpha| - R^\alpha}{K_v} \right\rangle^{n+1} + \frac{1}{2} \eta_\star^{-1}(\phi, \nabla\phi, \underset{\sim}{\boldsymbol{\kappa}})\, \overset{\times}{\underline{\boldsymbol{\sigma}}} \cdot \overset{\times}{\underline{\boldsymbol{\sigma}}}\,, \tag{68}$$

where $\langle \bullet \rangle = \mathrm{Max}(\bullet, 0)$ and τ^α is the resolved shear stress on slip system α that can be calculated as

$$\tau^\alpha = \underline{\boldsymbol{\ell}}^\alpha \cdot \underset{\sim}{\boldsymbol{\sigma}} \cdot \underline{\boldsymbol{n}}^\alpha\,, \tag{69}$$

where $\underline{\boldsymbol{\ell}}^\alpha$ and $\underline{\boldsymbol{n}}^\alpha$ are respectively the slip direction and normal to the slip plane. Note that the stress tensor is not symmetric so that a contribution to the resolved

shear stress arises from the double contraction of the skew–symmetric stress with the skew–symmetric part of the tensor $\underline{\boldsymbol{\ell}}^{\alpha} \otimes \underline{\boldsymbol{n}}^{\alpha}$. This contribution can be interpreted as a size–dependent kinematic hardening, as shown in [Sedláček and Forest, 2000; Sedláček *et al.*, 2002; Forest and Sedláček, 2003; Forest, 2008]. The second term in (68) is supposed to be active only in the grain boundary regions which can be achieved by constructing $\eta_{\star}(\phi, \nabla\phi, \underset{\sim}{\boldsymbol{\kappa}})$ in terms of its arguments so that it is small inside the grain boundaries and large inside the grains. The pseudo-vector $\overset{\times}{\underline{\boldsymbol{\sigma}}}$ contains the skew-symmetric contributions to the stress. The evolution of plastic deformation follows from (58) and (68)

$$\dot{\underset{\sim}{\boldsymbol{e}}}^{p} = \sum_{\alpha=1}^{N} \dot{\gamma}^{\alpha}\, \underline{\boldsymbol{\ell}}^{\alpha} \otimes \underline{\boldsymbol{n}}^{\alpha} + \eta_{\star}^{-1}(\phi, \nabla\phi, \underset{\sim}{\boldsymbol{\kappa}})\, \mathrm{skew}(\, \underset{\sim}{\boldsymbol{\sigma}}\,)\,, \tag{70}$$

with the slip rate given by

$$\dot{\gamma}^{\alpha} = \left\langle \frac{|\tau^{\alpha}| - R^{\alpha}}{K_v} \right\rangle^{n} \mathrm{sign}\, \tau^{\alpha}\,. \tag{71}$$

Whereas the first part of (70) is a classic crystal flow rule the second part is included to take into account the reorientation which takes place in the interface region during grain boundary migration as a result of atomic reshuffling processes. It is a purely skew-symmetric contribution, i.e. it acts only on the plastic spin. Specifically, the skew-symmetric plastic deformation can be written as

$$\overset{\times}{\underline{\boldsymbol{e}}}^{p} = \overset{\times}{\underline{\boldsymbol{e}}}^{slip} + \overset{\times}{\underline{\boldsymbol{e}}}^{\star}\,, \tag{72}$$

with

$$\dot{\overset{\times}{\underline{\boldsymbol{e}}}}^{slip} = \overset{\times}{\underline{\boldsymbol{\omega}}}^{p} - \overset{\times}{\underline{\boldsymbol{\omega}}}^{\star}\,, \qquad \underset{\sim}{\boldsymbol{\omega}}^{p} - \underset{\sim}{\boldsymbol{\omega}}^{\star} = \mathrm{skew}(\sum_{\alpha=1}^{N} \dot{\gamma}^{\alpha}\, \underline{\boldsymbol{\ell}}^{\alpha} \otimes \underline{\boldsymbol{n}}^{\alpha}\,)\,, \tag{73}$$

$$\dot{\overset{\times}{\underline{\boldsymbol{e}}}}^{\star} = \overset{\times}{\underline{\boldsymbol{\omega}}}^{\star}\,, \qquad \overset{\times}{\underline{\boldsymbol{\omega}}}^{\star} = \eta_{\star}^{-1}(\phi, \nabla\phi, \underset{\sim}{\boldsymbol{\kappa}})\, \overset{\times}{\underline{\boldsymbol{\sigma}}}\,. \tag{74}$$

The quantity $\overset{\times}{\underline{\boldsymbol{e}}}^{\star}$ which is here associated with the plastic spin was introduced in the form of an eigendeformation with an associated evolution law in [Ask *et al.*, 2018b]. In order to compare the two formulations, consider the elastic skew-symmetric deformation which is given by

$$\overset{\times}{\underline{\boldsymbol{e}}}^{e} = \overset{\times}{\underline{\boldsymbol{\vartheta}}}^{e} - \underline{\boldsymbol{\Theta}} = \overset{\times}{\underline{\boldsymbol{\vartheta}}} - \overset{\times}{\underline{\boldsymbol{e}}}^{p} - \underline{\boldsymbol{\Theta}} = \overset{\times}{\underline{\boldsymbol{\vartheta}}} - \overset{\times}{\underline{\boldsymbol{e}}}^{slip} - \overset{\times}{\underline{\boldsymbol{e}}}^{\star} - \underline{\boldsymbol{\Theta}}\,. \tag{75}$$

When the Cosserat microrotations are taken to represent the lattice orientation measured relative to a fixed frame, they are in general non-zero in the reference configuration. If the deformations are zero it must hold that $\overset{\times}{\underline{\boldsymbol{\vartheta}}}(t=0) = \underline{\mathbf{0}}$. In [Ask *et al.*, 2018b], this was resolved by adopting the following initial conditions

$$\overset{\times}{\underline{\boldsymbol{e}}}^{\star}(t=0) = -\underline{\boldsymbol{\Theta}}(t=0)\,. \tag{76}$$

The same assumption can be made in this case, however unlike in [Ask *et al.*, 2018b], this will also have as a consequence that

$$\overset{\times}{\underset{\sim}{e}}{}^{p}(t=0) = -\underline{\boldsymbol{\Theta}}(t=0)\,, \tag{77}$$

since here the skew-symmetric plastic deformation does not only contain the contribution due to plastic slip. Non-zero initial conditions on the plastic deformation were also adopted in [Admal *et al.*, 2018] in order to accommodate a polycrystal made of differently oriented grains.

From (75) it is clear that an evolution of the Cosserat microrotation due to a migrating grain boundary would result in a non-zero $\overset{\times}{\underset{\sim}{e}}{}^{e}$ and thereby a skew-symmetric stress in the region swept by the moving front. Due to (74), this stress is relaxed by evolution of $\overset{\times}{\underset{\sim}{e}}{}^{\star}$.

The evolution of the scalar dislocation densities ρ^{α} is assumed to follow a modified Kocks-Mecking-Teodosiu evolution law [Abrivard *et al.*, 2012a,b; Ask *et al.*, 2018b] such that

$$\dot{\rho}^{\alpha} = \begin{cases} \frac{1}{b}\left(K\sqrt{\sum_{\beta}\rho^{\beta}} - 2d\rho^{\alpha}\right)|\dot{\gamma}^{\alpha}| - \rho^{\alpha}\, C_D\, A(|\underset{\sim}{\boldsymbol{\kappa}}|)\,\dot{\phi} & \text{if } \dot{\phi} > 0 \\ \frac{1}{b}\left(K\sqrt{\sum_{\beta}\rho^{\beta}} - 2d\rho^{\alpha}\right)|\dot{\gamma}^{\alpha}| & \text{if } \dot{\phi} \leq 0 \end{cases} \tag{78}$$

The additional term compared to (32) accounts for static recovery due to dislocations being annihilated in the wake of a migrating grain boundary. Full recovery is obtained for sufficiently high values of the parameter C_D. The function $A(|\underset{\sim}{\boldsymbol{\kappa}}|)$ is chosen so that it localizes the static recovery process to the grain boundary regions.

The evolution of the phase field ϕ is chosen to be governed by a quadratic dissipation potential [Gurtin, 1996; Abrivard *et al.*, 2012a]

$$\Omega^{\phi} = \frac{1}{2}\eta_{\phi}^{-1}(\phi, \nabla\phi, {}^{\sharp}\underset{\sim}{\boldsymbol{\Gamma}}^{e})\,\pi_{\phi}^{neq2}\,, \tag{79}$$

so that

$$\eta_{\phi}(\phi, \nabla\phi, {}^{\sharp}\underset{\sim}{\boldsymbol{\Gamma}}^{e})\dot{\phi} = -\pi_{\phi}^{neq}\,. \tag{80}$$

5. Numerical solution of the triple junction problem

The model presented in the previous section has been implemented for numerical simulations by finite elements in the Z-set code [Z–set package, 2013]. Details on the numerical implementation can be found in [Ammar *et al.*, 2009; Ask *et al.*, 2018b]. Since the implementation is in two dimensions, rotation only takes place around one axis (in this case the $z-$axis) and the Cosserat pseudo-vector of microrotations only has one non-zero contribution θ such that $\underline{\boldsymbol{\Theta}} = [\,0\;0\;\theta\,]^{T}$. Figure 2 shows the geometry of the triple junction problem. Dirichlet conditions are assumed for ϕ, θ and the displacements $\underline{\boldsymbol{u}}$, with $u_x = u_y = 0$ along the boundaries. The computational domain is assumed to be $10 \times 10\ \mu\text{m}^2$ and is discretized by 50×50 quadratic elements

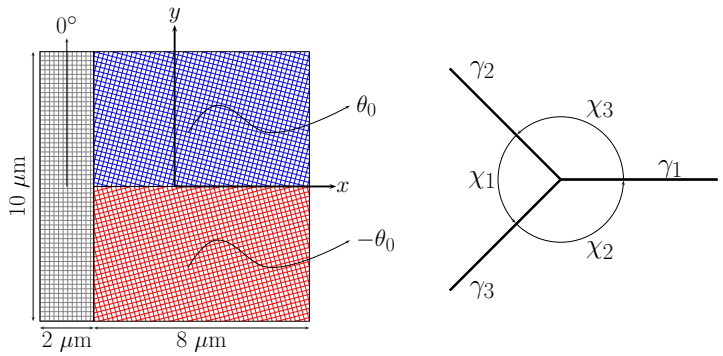

Fig. 2. Geometry and initial conditions for the triple junction problem (left) and definition of angles and grain boundaries for the Herring's equation (right).

with reduced integration. The simulations are performed on a non-dimensionalized system according to Ask *et al.* [2018b], with $\overline{x} = x/\Lambda$ and $\overline{y} = y/\Lambda$ where $\Lambda = 1$ μm. The term $\eta_\star(\phi, \nabla\phi, \underset{\sim}{\boldsymbol{\kappa}})$ in (74) is taken to be

$$\eta_\star(\nabla\theta) = \hat{\eta}_\star \left[1 - \left[1 - \frac{\mu_p}{\varepsilon}\right] \exp(-\beta_P \, \varepsilon \, |\nabla\theta|)\right] , \tag{81}$$

with the coefficients chosen such that $\mu_p/\varepsilon = 1000$ and $\beta_P \, \varepsilon = 1000$.

The model parameters are given in 1. Values that are reasonable for pure copper have been chosen although a formal fit to experimental data has not been carried out. Dimensionless time $\bar{t} = t/\tau_0$ is used in the simulations. A physical time scale can be set by choosing the parameter τ_0. Initial conditions must be provided for ϕ, θ and the viscoplastic pseudo–vector $\overset{\times}{\underline{\boldsymbol{e}}}^\star$. The initial fields $\phi(\bar{t} = 0)$ and $\theta(\bar{t} = 0)$ are constructed by means of sinh and tanh functions, respectively, whereas $\overset{\times}{\underline{\boldsymbol{e}}}^\star$ is initialized so that $\overset{\times}{\underline{\boldsymbol{e}}}^e(\bar{t} = 0) = \underline{\mathbf{0}}$.

Table 1. Model parameters.

	f_0	a	s	ε	η_ϕ	$\hat{\eta}_\star$	μ	λ	μ_c
Unit	[MPa]	[μm]	[μm]	[μm]	[MPa s]	[MPa s]	[GPa]	[GPa]	[GPa]
Value	1.8	0.3	2.	2.	0.1 $f_0 \, \tau_0$	0.1 $f_0 \, \tau_0$	46.1	69.2	1.8

5.1. *Equilibrium of the triple junction*

In two dimensions the triple junction problem concerns finding the equilibrium solution when three grains have a common intersection. The solution will be of the format shown schematically in figure 2 (right). If the grain boundary energies γ_i are known, the Herring equation [Herring, 1951] can be used to calculate the corresponding angles of the intersection according to

$$\frac{\gamma_1}{\sin(\chi_1)} = \frac{\gamma_2}{\sin(\chi_2)} = \frac{\gamma_3}{\sin(\chi_3)} \, . \tag{82}$$

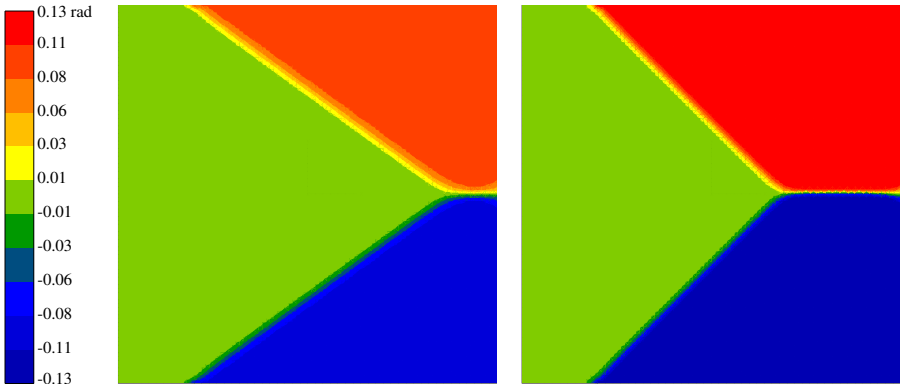

Fig. 3. The equilibrium solution with $\theta_0 = \pm 5^\circ$ (left) and $\theta_0 = \pm 7.5^\circ$ (right). It is evident from the images that the angles of the triple junction are different for the different grain misorientations. Due to the diffuse nature of the interfaces and the discrete finite element mesh, the exact point of the triple junction and thereby the angles can only be measured approximately. For $\theta_0 = \pm 5^\circ$, the triple junction is at approximately $\overline{x} = 4 \pm 0.1$ and for $\theta_0 = \pm 7.5^\circ$, it is at approximately $\overline{x} = 2 \pm 0.1$ (origin is at the center of the computational domain).

Note that only for equal grain boundary energies (which would be the case for equal misorientation between all grains) the angles χ_i are equal and each 120°. Here, an initial geometry according to figure 2 will be used, with the left-hand side grain having an initial orientation of 0° and the other two grains $\pm\theta_0$. This will result in two identical angles $\chi_2 = \chi_3$ and some manipulation of equation (82) results in

$$\cos(\chi_2) = -\frac{1}{2}\frac{\gamma_1}{\gamma_2}\,, \tag{83}$$

with $\chi_1 = 360^\circ - 2\,\chi_2$.

The corresponding grain boundary energies for the chosen misorientations θ_0 can be calculated using the results of asymptotic expansion of the orientation phase field model by Lobkovsky and Warren [2001]. The derivation of the asymptotic solution is rather long and will not be repeated here, the reader is referred to [Ask *et al.*, 2018b] for more details. Due to the strongly coupled nature of the two fields ϕ and θ in the model, the solution in the sharp interface limit must be resolved numerically. The calculated *dimensionless* grain boundary energies $\overline{\gamma}_1$ and $\overline{\gamma}_2$ for $\theta_0 = \pm 7.5^\circ$ and $\theta_0 = \pm 5^\circ$ are given in table 2, together with the corresponding angle χ_2 calculated from (83).

Figure 3 shows the equilibrium solutions for $\theta_0 = \pm 5^\circ$ (left) and $\theta_0 = \pm 7.5^\circ$ (right). It is evident from the figure that different misorientations result in different angles χ_i, as expected. Due to the diffuse nature of the interfaces and the discrete finite element mesh, the exact point of the triple junction and thereby the angles can only be measured approximately. For $\theta_0 = \pm 5^\circ$, the triple junction is at approximately $\overline{x}_{TP} = 4$ and for $\theta_0 = \pm 7.5^\circ$, it is at approximately $\overline{x}_{TP} = 2$ (the origin is at the center of the computational domain). With the initial geometry given by figure 2, and recalling that Dirichlet boundary conditions are used, the angle χ_2

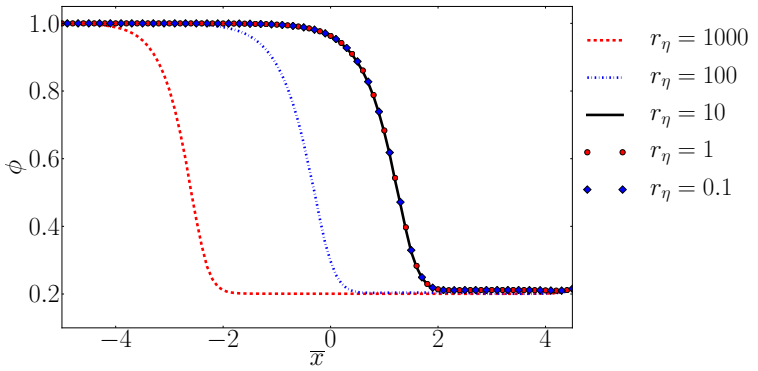

Fig. 4. The influence of the parameter $\hat{\eta}_\star$ on the mobility of the grain boundaries. The figure shows the profile of the phase field ϕ along $\overline{y} = 0$ at $\overline{t} = 10$ for different ratios $r_\eta = \hat{\eta}_\star/\eta_\phi$. The triple junction is approximately positioned where the gradient of the phase field is maximum.

found in the simulations can then be calculated as

$$\chi_2 \approx \arctan((\overline{x}_{TP} + 3)/5) + \pi/2\,. \tag{84}$$

The resulting approximate values for χ_2 are presented in table 2. The agreement is very good between the (semi-)analytic results and the simulations.

Table 2. Solution to the Herring equilibrium and numerical (FE) results.

$\pm\theta_0$	$\overline{\gamma}_1$	$\overline{\gamma}_2$	χ_2	$\overline{x}_{TP}$	χ_2 (FE)
5°	0.115	0.071	144°	4 ± 0.1	$144.5° \pm 0.3°$
7.5°	0.138	0.096	136°	2 ± 0.1	$135° \pm 0.6°$

5.2. *Parameter study and grain boundary mobility*

In the proposed coupled model there is no separate relaxational dynamics for θ. Instead, local reorientation in the grain boundary to allow for migration is made possible by the evolution law for the plastic deformation and specifically the plastic spin term $\underset{\sim}{\boldsymbol{\omega}}^\star$. Ideally, the mobility of the grain boundary should be determined only by the phase field relaxational (mobility) parameter η_ϕ. However, if the relaxation of the plastic spin is too slow, this will slow down or prevent the grain boundary from migrating.

Simulations where carried out with $\hat{\eta}_\star$ varying by several orders of magnitude in order to study its impact on the grain boundary migration. The other model parameters are those in table 1. For the angles, $\theta_0 = \pm 7.5°$ was used. Note that the absolute value of $\hat{\eta}_\star$ is of less interest than the ratio $r_\eta = \hat{\eta}_\star/\eta_\phi$. Measuring the exact position of the triple junction during the simulations is not practical,

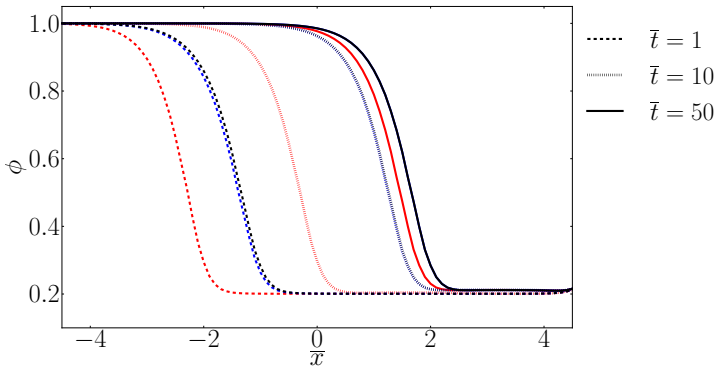

Fig. 5. The influence of the parameter $\hat{\eta}_\star$ on the mobility of the grain boundaries. The figure shows the profile of ϕ along $\overline{y} = 0$ at $\overline{t} = 1, 10$ and 50 for $r_\eta = 100$ (red lines) $r_\eta = 10$ (black lines) and $r_\eta = 1$ (blue lines). For $\overline{t} = 10$ and 50 black and blue lines overlap.

instead the profile of the phase field ϕ along $\overline{y} = 0$ is traced over time for different values of r_η. The triple junction is approximately positioned where the gradient of the phase field is maximum. In figure 4, the profile of ϕ along $\overline{y} = 0$ at $\overline{t} = 10$ is shown for $r_\eta = 1000, 100, 10, 1$ and 0.1, respectively. For all $r_\eta \leq 10$, the same profile is recovered. Figure 5 shows the the profile of ϕ along $\overline{y} = 0$ at $\overline{t} = 1, 10$ and 50 for $r_\eta = 100$ (red lines) $r_\eta = 10$ (black lines) and $r_\eta = 1$ (blue lines). Again, there is not much difference between $r_\eta = 10$ and $r_\eta = 1$. This gives an indication that, provided $\hat{\eta}_\star$ is chosen sufficiently small with respect to η_ϕ, this parameter does not influence the grain boundary mobility. Similar results were found by Ask *et al.* [2018b], however in that work there was an additional relaxational equation for the Cosserat orientation which is not included here. This feature makes the model simpler for practical use compared to the original KWC formulation.

5.3. *Stresses in the grain boundary*

Figure 6 shows the evolution of the triple junction over time, from left to right $\overline{t} = 0.1, 1, 10$ and 50. The phase field ϕ is shown in the top row and the orientation θ in the bottom row. A misorientation of $\theta_0 = \pm 7.5°$ was used together with the material parameters in table 1. It appears that the correct angles χ_i are stabilized first and then the triple point migrates to minimize the grain boundary curvature.

The grain boundary migration is not expected to give rise to any significant strains in the simulations for the triple junction problem. However, there are still stresses present. The microstress π_ϕ which belongs to the phase field ϕ and is given by equation (63) is non-zero in the grain boundary region. The dissipative part of this stress drives the evolution of ϕ according to (80). The progress of the microstress π_ϕ over time is shown in figure 7.

When the grain boundaries migrate and the orientation changes, the skew-symmetric stress $\overset{\times}{\underline{\boldsymbol{\sigma}}}$ becomes non-zero. This in turn drives the evolution of $\underset{\sim}{\boldsymbol{\omega}}^\star$ which

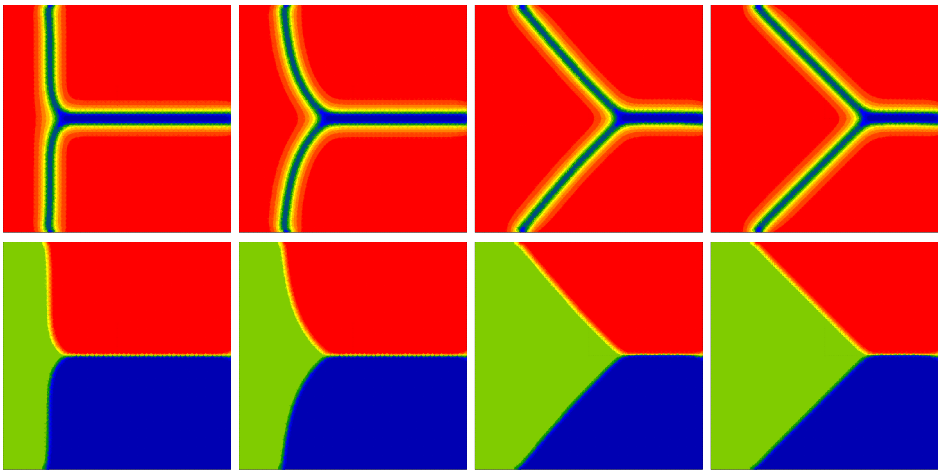

Fig. 6. Evolution of the triple junction over time, from left to right $\bar{t} = 0.1, 1, 10$ and 50. The top plots show $\phi \in [0, 1]$ and the bottom plots show $\theta \in [-7.5°, 7.5°]$.

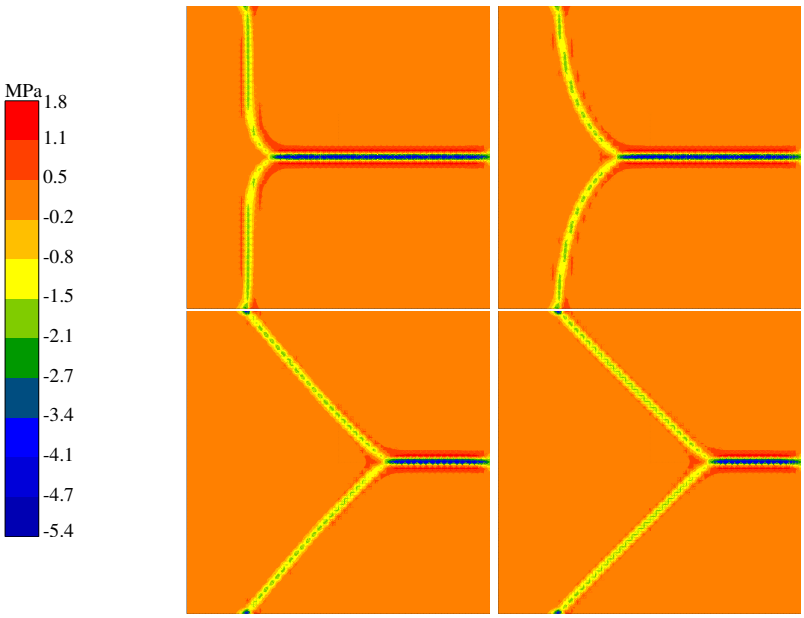

Fig. 7. Microstress $\pi_\phi \in [-5.4, 1.8]$ inside the grain boundary at time $\bar{t} = 0.1, 1, 10$ and 50 (left to right, top to bottom). Note that as the solution stabilizes, the dissipative part π_ϕ^{neq} goes to zero and only the energetic contribution remains.

relaxes the skew-symmetric stress and allows for the grain boundary to migrate. In the two dimensional simulations, there is only one non-zero contribution $\overset{\times}{\sigma} = \overset{\times}{\sigma}_3$ to $\underline{\overset{\times}{\boldsymbol{\sigma}}}$. The rate at which the skew-symmetric stress vanishes depends on the parameter $\hat{\eta}_\star$. If this viscosity type parameter is large relative to the parameter η_ϕ which

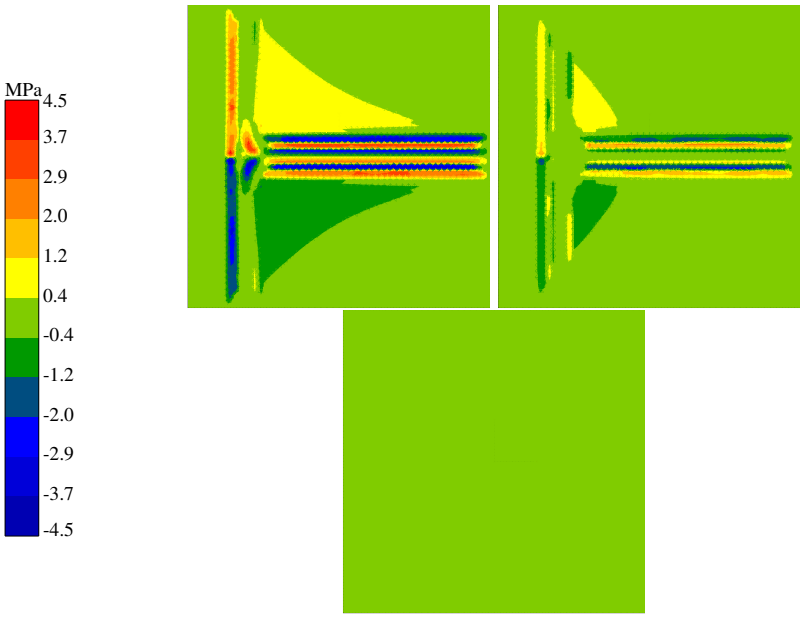

Fig. 8. skew-symmetric stress contribution $\overset{\times}{\sigma}$ at $\bar{t} = 0.1$ for three different values of $r_\eta = \hat{\eta}_\star/\eta_\phi$. From left to right, top to bottom: $r_\eta = 100$, 10 and 1.

controls the grain boundary mobility, the stress does not have time to relax and it remains, slowing down the grain boundary migration as evidenced by the fact that a larger ratio $r_\eta = \hat{\eta}_\star/\eta_\phi$ implies a slower evolution towards equilibrium. The effect of the parameter $\hat{\eta}_\star$ is demonstrated in figure 8 which shows the skew-symmetric stress contribution $\overset{\times}{\sigma}$ at $\bar{t} = 0.1$ for three different values of $r_\eta = \hat{\eta}_\star/\eta_\phi$. In particular, for $r_\eta = 1$, the skew-symmetric stress has already relaxed after $\bar{t} = 0.1$.

By construction, the choice of the viscosity type parameter $\hat{\eta}_\star$ influences the relaxation time for the skew-symmetric stress in the grain boundaries. It is demonstrated that this in turn plays a role for the grain boundary migration which is slowed down if the skew-symmetric stress does not relax sufficiently fast.

6. Summary and outlook

The coupling of phase field and mechanical models for the simulation of grain boundary migration under load still is a largely open theoretical question. The most popular multiphase field approach does not properly account for the role of the development of lattice curvature inside the grains in recrystallization processes. In the present work, the full coupling is performed within the Cosserat mechanical framework thus extending the KWC approach. A slightly modified version of the coupled crystal plasticity-phase field model proposed in [Ask *et al.*, 2018b] was presented. By a short review of the underlying theory, the motivation for using an

orientation phase field model together with the Cosserat crystal plasticity theory was elaborated. The coupling between the orientation phase field model and the Cosserat theory is very natural as they both contain orientation as a degree of freedom. The model has earlier been demonstrated to have the ability to predict grain boundary migration due to both grain boundary energy and stored energy gradients due to scalar dislocation densities. In this work it was demonstrated that the model correctly predicts the equilibrium solution to the well-known triple junction problem. It was also demonstrated how the material parameters may influence the grain boundary migration and for which choices of material parameters skew-symmetric stresses in the grain boundary vanish or remain and counteract grain boundary mobility, respectively.

The coupling of a higher order crystal plasticity theory and an orientation phase field model was also successfully pursued by Admal *et al.* [2018]. Although the formulations are not identical and have been applied to slightly different problems of coupled deformation and grain boundary migration, it is clear that this type of modeling framework is promising and represents a major step toward a truly unified theory applicable to microstructure evolution during deformation and recrystallization processes.

The finite deformation theory of the model is the subject of the work [Ask *et al.*, 2018a]. Its corresponding numerical implementation is a challenging task which will make possible the simulation of processes such as cold rolling involving very large plastic strains and lattice rotation and curvature. It should also be noted that although the model is presented for isothermal conditions in this work (for brevity), temperature effects remain to be incorporated at various suitable places in the model.

Acknowledgements

This project has received funding from the European Research Council (ERC) under the European Union's Horizon 2020 research and innovation program (grant agreement n° 707392 MIGRATE).

References

Abrivard, G., Busso, E. P., Forest, S. and Appolaire, B. [2012a] "Phase field modelling of grain boundary motion driven by curvature and stored energy gradients. Part I: theory and numerical implementation," *Philosophical Magazine* **92**, 3618–3642.

Abrivard, G., Busso, E. P., Forest, S. and Appolaire, B. [2012b] "Phase field modelling of grain boundary motion driven by curvature and stored energy gradients. Part II: Application to recrystallisation," *Philosophical Magazine* **92**, 3643–3664.

Admal, N. C., Po, G. and Marian, J. [2018] "A unified framework for polycrystal plasticity with grain boundary evolution," *International Journal of Plasticity* doi:https://doi.org/10.1016/j.ijplas.2018.01.014, URL http://www.sciencedirect.com/science/article/pii/S0749641917305557.

Allen, S. M. and Cahn, J. W. [1979] "A microscopic theory for antiphase boundary motion and its application to antiphase domain coarsening," *Acta Metallurgica* **27**(6), 1085–1095.

Ammar, K., Appolaire, B., Cailletaud, G., Feyel, F. and Forest, S. [2009] "Finite element formulation of a phase field model based on the concept of generalized stresses," *Computational Materials Science* **45**, 800–805.

Ashby, M. [1970] "The deformation of plastically non–homogeneous materials," *Philosophical Magazine* **21**, 399–424.

Ask, A., Forest, S., Appolaire, B. and Ammar, K. [2018a] "A cosserat–phase field theory of crystal plasticity and grain boundary migration at finite deformation," *submitted to Continuum Mechanics and Thermodynamics* .

Ask, A., Forest, S., Appolaire, B., Ammar, K. and Salman, O. U. [2018b] "A cosserat crystal plasticity and phase field theory for grain boundary migration," *Journal of the Mechanics and Physics of Solids* **115**, 167–194, doi: https://doi.org/10.1016/j.jmps.2018.03.006.

Blesgen, T. [2014] "Deformation patterning in three-dimensional large-strain Cosserat plasticity," *Mechanics Research Communications* **62**, 37 – 43.

Blesgen, T. [2017] "A variational model for dynamic recrystallization based on Cosserat plasticity," *Composites Part B: Engineering* **115**, 236–243.

Cermelli, P. and Gurtin, M. E. [2001] "On the characterization of geometrically necessary dislocations in finite plasticity," *Journal of the Mechanics and Physics of Solids* **49**(7), 1539–1568.

Chuan, W., He, Y. and Wei, L. H. [2013] "Modeling of discontinuous dynamic recrystallization of a near-α titanium alloy imi834 during isothermal hot compression by combining a cellular automaton model with a crystal plasticity finite element method," *Computational Materials Science* **79**, 944–959.

Cordero, N. M., Forest, S., Busso, E. P., Berbenni, S. and Cherkaoui, M. [2012] "Grain size effects on plastic strain and dislocation density tensor fields in metal polycrystals," *Computational Materials Science* **52**, 7–13.

Cosserat, E. and Cosserat, F. [1909] *Théorie des corps déformables* (Hermann, Paris).

Eringen, A. C. [1976] "Polar and nonlocal field theories," in A. C. Eringen (ed.), *Continuum Physics. Vol 4.* (Academic Press, London).

Eringen, A. C. and Kafadar, C. B. [1976] "Part I. Polar Field Theories," in A. C. Eringen (ed.), *Continuum Physics* (Academic Press), pp. 1–73.

Fleck, N. and Hutchinson, J. [1997] "Strain gradient plasticity," *Adv. Appl. Mech.* **33**, 295–361.

Forest, S. [2008] "Some links between Cosserat, strain gradient crystal plasticity and the statistical theory of dislocations," *Philosophical Magazine* **88**, 3549–3563.

Forest, S., Barbe, F. and Cailletaud, G. [2000] "Cosserat modelling of size effects in the mechanical behaviour of polycrystals and multiphase materials," *International Journal of Solids and Structures* **37**, 7105–7126.

Forest, S., Boubidi, P. and Sievert, R. [2001] "Strain localization patterns at a crack tip in generalized single crystal plasticity," *Scripta Materialia* **44**, 953–958.

Forest, S., Cailletaud, G. and Sievert, R. [1997] "A Cosserat theory for elastoviscoplastic single crystals at finite deformation," *Archives of Mechanics* **49**(4), 705–736.

Forest, S. and Guéninchault, N. [2013] "Inspection of free energy functions in gradient crystal plasticity," *Acta Mechanica Sinica* **29**, 763–772.

Forest, S. and Sedláček, R. [2003] "Plastic slip distribution in two–phase laminate microstructures: Dislocation–based vs. generalized–continuum approaches," *Philosophical Magazine A* **83**, 245–276.

Forest, S. and Sievert, R. [2003] "Elastoviscoplastic constitutive frameworks for generalized continua," *Acta Mechanica* **160**, 71–111.

Franciosi, P., Berveiller, M. and Zaoui, A. [1980] "Latent hardening in copper and aluminium single crystals," *Acta Metallurgica* **28**(3), 273–283.

Gottstein, G. and Shvindlerman, L. [2010] *Grain boundary migration in metals* (CRC Press, Berlin).

Gurtin, M. E. [1996] "Generalized Ginzburg-Landau and Cahn-Hilliard equations based on a microforce balance," *Physica D: Nonlinear Phenomena* **92**(3), 178–192.

Gurtin, M. E. [2002] "A gradient theory of single-crystal viscoplasticity that accounts for geometrically necessary dislocations," *Journal of the Mechanics and Physics of Solids* **50**(1), 5–32.

Gurtin, M. E. and Lusk, M. T. [1999] "Sharp-interface and phase-field theories of recrystallization in the plane," *Physica D: Nonlinear Phenomena* **130**(1–2), 133–154.

Güvenç, O., Bambach, M. and Hirt, G. [2014] "Coupling of crystal plasticity finite element and phase field methods for the prediction of SRX kinetics after hot working," *steel research international* **85**(6), 999–1009.

Güvenç, O., Henke, T., Laschet, G., Böttger, B., Apel, M., Bambach, M. and Hirt,

G. [2013] "Modelling of static recrystallization kinetics by coupling crystal plasticity FEM and multiphase field calculations," *Computer Methods in Materials Science* **13**(2), 368–374.

Herring, C. [1951] "Some theorems on the free energies of crystal surfaces," *Physical Review* **82**, 87–93.

Humphreys, F. and Hatherly, M. [2004] *Recrystallization and Related Annealing Phenomena* (Elsevier).

Kobayashi, R. and Giga, Y. [1999] "Equations with Singular Diffusivity," *Journal of Statistical Physics* **95**(5-6), 1189–1220.

Kobayashi, R., Warren, J. A. and Carter, W. C. [2000] "A continuum model of grain boundaries," *Physica D* **140**(1-2), 141–150.

Kocks, U. F. and Mecking, H. [2003] "Physics and phenomenology of strain hardening: the FCC case," *Progress in Materials Science* **48**, 171–273.

Kröner, E. [1959] "Allgemeine Kontinuumstheorie der Versetzungen und Eigenspannungen," *Archive for Rational Mechanics and Analysis* **4**, 273–334.

Lee, E. H. [1969] "Elastic-plastic deformation at finite strains," *Journal of Applied Mechanics* **36**, 1–6.

Lobkovsky, A. E. and Warren, J. A. [2001] "Sharp interface limit of a phase-field model of crystal grains," *Physical Review E* **63**(5), 051605.

Mandel, J. [1972] *Plasticité classique et viscoplasticité, CISM Courses and Lectures No. 97, Udine, 1971* (Springer-Verlag).

Mandel, J. [1973] "Equations constitutives et directeurs dans les milieux plastiques et viscoplastiques," *Int. J. Solids Structures* **9**, 725–740.

Mayeur, J. and McDowell, D. [2014] "A comparison of gurtin type and micropolar theories of generalized single crystal plasticity," *International Journal of Plasticity* **57**, 29–51, doi:http://dx.doi.org/10.1016/j.ijplas.2014.01.010.

Mayeur, J., McDowell, D. and Bammann, D. [2011] "Dislocation–based micropolar single crystal plasticity: Comparison of multi– and single criterion theories," *Journal of the Mechanics and Physics of Solids* **59**, 398–422.

Mellbin, Y., Hallberg, H. and Ristinmaa, M. [2017] "An extended vertex and crystal plasticity framework for efficient multiscale modeling of polycrystalline materials," *International Journal of Solids and Structures* **125**, 150 – 160, doi:https://doi.org/10.1016/j.ijsolstr.2017.07.009.

Mesarovic, S. D., Forest, S. and Jaric, J. P. [2015] "Size-dependent energy in crystal plasticity and continuum dislocation models," *Proceedings of the Royal Society A: Mathematical, Physical and Engineering Sciences* **471**(2175), 20140868, 19 p.

Nye, J. [1953] "Some geometrical relations in dislocated crystals," *Acta Metall.* **1**, 153–162.

Ohno, N. and Okumura, D. [2007] "Higher–order stress and grain size effects due to self–energy of geometrically necessary dislocations," *Journal of the Mechanics and Physics of Solids* **55**, 1879–1898.

Raabe, D. and Becker, R. C. [2000] "Coupling of a crystal plasticity finite-element model with a probabilistic cellular automaton for simulating primary static recrystallization in aluminium," *Modelling and Simulation in Materials Science and Engineering* **8**(4), 445.

Rollett, A. [1997] "Overview of modeling and simulation of recrystallization," *Progress in Materials Science* **42**(1), 79–99.

Sedláček, R., Blum, W., Kratochvil, J. and Forest, S. [2002] "Subgrain formation during deformation : physical origin and consequences," *Metallurgical and Materials Transactions* **33A**, 319–327.

Sedláček, R. and Forest, S. [2000] "Non-local plasticity at microscale : A dislocation-based model and a Cosserat model," *physica status solidi (b)* **221**, 583–596.

Steinbach, I. [2009] "Phase-field models in materials science," *Modelling and Simulation in Materials Science and Engineering* **17**(7), 073001.

Steinbach, I. and Pezzolla, F. [1999] "A generalized field method for multiphase transformations using interface fields," *Physica D: Nonlinear Phenomena* **134**(4), 385–393.

Steinbach, I., Pezzolla, F., Nestler, B., Seeßelberg, M., Prieler, R., Schmitz, G. J. and Rezende, J. L. L. [1996] "A phase field concept for multiphase systems," *Physica D: Nonlinear Phenomena* **94**(3), 135–147.

Takaki, T., Hisakuni, Y., Hirouchi, T., Yamanaka, A. and Tomita, Y. [2009] "Multi-phase-field simulations for dynamic recrystallization," *Computational Materials Science* **45**(4), 881–888.

Takaki, T. and Tomita, Y. [2010] "Static recrystallization simulations starting from predicted deformation microstructure by coupling multi-phase-field method and finite element method based on crystal plasticity," *International Journal of Mechanical Sciences* **52**(2), 320–328.

Takaki, T., Yamanaka, A., Higa, Y. and Tomita, Y. [2007] "Phase-field model during static recrystallization based on crystal-plasticity theory," *Journal of Computer-Aided Materials Design* **14**(1), 75–84.

Taylor, G. I. [1934] "The mechanism of plastic deformation of crystals. part i.—theoretical," *Proceedings of the Royal Society of London A: Mathematical, Physical and Engineering Sciences* **145**(855), 362–387.

Teodosiu, C. and Sidoroff, F. [1976] "A theory of finite elastoviscoplasticity of single crystals," *International Journal of Engineering Science* **14**, 165–176.

Vondrous, A., Bienger, P., Schreijäg, S., Selzer, M., Schneider, D., Nestler, B., Helm, D. and Mönig, R. [2015] "Combined crystal plasticity and phase-field method for recrystallization in a process chain of sheet metal production," *Computational Mechanics* **55**(2), 439–452.

Warren, J. A., Kobayashi, R., Lobkovsky, A. E. and Carter, W. C. [2003] "Extending phase field models of solidification to polycrystalline materials," *Acta Materialia* **51**(20), 6035–6058.

Wulfinghoff, S., Forest, S. and Böhlke, T. [2015] "Strain gradient plasticity modeling

of the cyclic behavior of laminate microstructures," *Journal of the Mechanics and Physics of Solids* **79**, 1–20, doi:10.1016/j.jmps.2015.02.008.

Z–set package [2013] "Non-linear material & structure analysis suite, www.zset-software.com," .